Contrasting the termination of moderate and extreme El Niño events in Coupled General Circulation Models

Matthieu Lengaigne[1]

Gabriel A. Vecchi[2]

[1]Laboratoire d'Oceanographie et de Climatologie : Experimentations et Approches Numériques, Paris, France

[2]NOAA/Geophysical Fluid Dynamics Laboratory, Princeton, New Jersey, U.S.A

Submitted to Climate Dynamics

Corresponding author:

Matthieu Lengaigne

LOCEAN,
Couloir 45-55, 4ème étage
Case 100
4 place Jussieu
75252 Paris Cedex 05, France
Email: lengaign@lodyc.jussieu.fr
Tel : 0033.(0)1.44.27.70.76
Fax : 0033.(0)1.44.27.38.05

ABSTRACT

An assessment of coupled IPCC-AR4 models indicates that the termination characteristics and mechanisms of observed El Niño events, involving meridional processes tied to the seasonal cycle, are present in climate models. This includes the processes that precondition the termination of El Niño events in general, and the mechanisms leading to a peculiar termination of extreme El Niño events (such as those of 1982-3 and 1997-8), in which the eastern equatorial Pacific warm Sea Surface Temperature Anomalies (SSTA) persist well into boreal spring/early-summer. The mechanisms controlling the peculiar termination of extreme El Niño events, related to the development of an equatorially-centred intertropical convergence zone, are consistent across the four models that exhibit extreme El Niño events and observational record, suggesting that this peculiar termination represents a general feature of extreme El Niño events. Further, due to their unusual termination, extreme El Niño events exhibit an apparent eastward propagation of their SSTA, which can strongly influence estimates of the apparent propagation of ENSO over multi-decadal periods. Interpreting these propagation changes as evidence of changes in the underlying dynamical feedbacks behind El Niño could therefore be misleading, given the strong influence of a single extreme event.

Keywords: El Niño/Southern Oscillation (ENSO), extreme events, IPCC-AR4 climate models, coupled ocean-atmosphere mechanisms, validation

1. **Introduction**

The El Niño/Southern Oscillation (ENSO) phenomenon is a dominant mode of climate variability on interannual time scales, and impacts weather patterns across the globe. The physical processes behind ENSO that involve coupling between the ocean and atmosphere in the tropical Pacific have been studied intensively over the past decades (*e.g.*, Neelin *et al.* 1998 and Wang and Picaut 2004 for reviews). As the El Niño impacts strongly vary between events, depending on the characteristics of the warming (*e.g.,* McPhaden *et al.* 2006), it is essential to better understand the mechanisms controlling its evolution. Although the amplitude and spatial structure can vary considerably from one warm ENSO (El Niño) event to another, a robust feature of El Niño is the tendency to peak to in boreal winter (Rasmusson and Carpenter 1982; Harrison and Larkin 1998). Here we contrast the evolution of extreme and moderate El Niño events, with particular focus on the timing of and physical processes behind their peak and termination.

Figure 1 illustrates the characteristics of El Niño events that are the focus of this manuscript by showing the evolution of near-Equatorial conditions averaged over for extreme (left panels) and moderate (right panels) El Niño events over the ERA40 period (1957-2002). Moderate and extreme El Niño events both exhibit (by definition) warm sea surface temperature anomalies (SSTAs) across the eastern equatorial Pacific (EPAC); these warm SSTAs result in an eastward displacement of the west Pacific warm pool and are associated with increased precipitation in the central Pacific and a rainfall deficit in the western equatorial Pacific. The El Niño events exhibit westerly (positive) wind stress anomalies in the western and central equatorial Pacific prior to the onset of warm EPAC SSTAs (Rasmusson and Carpenter 1982;

Harrison and Larkin 1998; Vecchi and Harrison 2000). These westerlies generally arise as episodic bursts (Giese and Harrison 1991; Harrison and Vecchi 1997), are associated with changes in atmospheric convection (*e.g.*, Lengaigne et al 2003) and drive oceanic changes that develop and maintain the El Niño warm SSTAs (Giese and Harrison 1991; Lengaigne et al. 2002 ; Boulanger et al. 2003, Belamari et al. 2003).

In moderate El Niño events, the warmest surface waters (*e.g.* the 28°C isotherm in present climate) remain close to the Dateline throughout the event, with precipitation anomalies mainly in the western Pacific (Fig. 1.d-e), SSTAs achieve their peak amplitude in December, the peak warm SST anomalies decay by March of Year(+1) and are centered between the Dateline and 140°W. The maximum westerly wind anomalies of moderate El Niño events are confined to the western part of the basin, and decay at the end of Year(0). EPAC zonal winds remain easterly throughout the El Niño event, even exhibiting easterly anomalies east of 140°W for most of the El Niño event (Fig. 1.f).

In contrast, the composite of two strongest El Niño events have both the warmest surface waters and precipitation anomalies extending to the coast of South America in winter and spring of Year(0)-Year(+1). East Pacific warm SSTAs exhibit two distinct peaks, one centered around 110°W in winter and a second peak evident along the coast of South America in boreal spring of Year(+1); these fluctuations in SSTA occur without much change in absolute SSTs, which remain relatively constant close to 29°C, so the SSTA variations reflect the absence/delay of the seasonal cycle. The eastern edge of the positive precipitation anomalies displays an apparent eastward propagation across the Pacific, reaching the eastern boundary by January of Year (+1); and the positive precipitation anomalies abruptly disappear in late-spring of Year(+1) (Fig. 1c). The maximum westerly wind anomalies also propagate across the basin to the coast of South America, resulting in a disappearance of the equatorial easterlies in the eastern part of the basin in

boreal Spring of Year(+1). These characteristics are evident in each El Niño event, not just on average.

Both moderate and extreme El Niño events show a decrease in their near-Dateline westerly wind anomalies at the end of Year(+0) (Fig. 1b and Fig. 1d, Rasmusson and Carpenter 1982; Harrison 1987; Harrison and Larkin 1998). As shown on Figure 2, this decrease can be attributed to the southward shift of westerly anomalies in the western-central Pacific, away from the oceanic equatorial waveguide for both type of events. This southward shift has already been documented in observations (Harrison and Vecchi 1999; Vecchi and Harrison 2003) and is actually associated with the coupled response to seasonal changes in insolation (Vecchi and Harrison 2003; Spencer 2004; Lengaigne *et al.* 2006; Vecchi 2006; Xiao and Mechoso 2008). This reduction in westerly anomalies has been shown to drive the subsequent shoaling of the EPAC thermocline, preconditioning the termination of the El Niño event (Harrison and Vecchi 1999, Vecchi and Harrison 2003, Lengaigne et al 2006). For the moderate events, the thermocline shoaling leads to a decrease in SST (Harrison and Vecchi 2001, Zelle *et al.* 2004), since equatorial easterlies are present throughout the event and upwell the cooling signal into the mixed-layer.

However, during extreme El Niño event, the timing of the cooling in EPAC SSTs is not set (only preconditioned) by the thermocline shoaling. An analysis of the termination of the 1997-8 event illustrates the processes at play (Vecchi and Harrison 2006, Vecchi 2006). As the EPAC thermocline shoals, the local easterly winds disappear, decoupling the cooling subsurface from the surface; only when the easterlies return in late spring of Year(+1) does the return of upwelling leads to a sharp cooling of SSTs. The disappearance of the easterlies has been attributed to the development of an equatorial InterTropical Convergence Zone (ITCZ), and the return of easterlies to the subsequent northward retreat of the equatorial ITCZ. It was suggested

that this development and retreat of an equatorial ITCZ should be a general feature of extreme El Niño events, and it was hypothesized that the ITCZ movement was tied to the seasonal march of insolation and the presence of warm SST anomalies of sufficient intensity to place the warmest waters on Equator.

Thus, processes that are meridional in nature and tied to the seasonal cycle, have been suggested as fundamental to the termination of El Niño events: the southward shift of near-Dateline westerly anomalies preconditions the termination of El Niño events, and the development/retreat of an equatorial ITCZ prolongs and abruptly terminates extreme El Niño events.

Here we show that the mechanisms controlling the peculiar termination of extreme events in 1997-8 and 1982-3 are active in a suite of state-of-the-art global climate models. These results confirm that this peculiar termination is likely to occur with observed extreme El Niño events in general. Implications related to SSTA eastward/wesward propagating signals associated with this peculiar termination are also discussed. We suggest that the prolonged EPAC warm anomalies lead to an apparent eastward propagation of the termination of extreme events, which accounts for a large part of the eastward propagating SSTA signal associated with ENSO during the recent decades (1976-2000). The paper is structured as follows: Section 2 describes the IPCC database used, the differences between the termination of extreme and moderate El Niño events in this database and the mechanisms explaining these differences. Section 3 discusses the implications related to SSTA eastward/wesward propagating signals of the peculiar termination of extreme El Niño events. Finally, Section 4 presents a summary and discussion of the results.

2. Extreme and moderate El Niño events in CGCMs

2.1. Multi-model database

The simulations analysed in this paper are largely from models available via the Intergovernmental Panel on Climate Change Fourth Assessment Report (IPCC-AR4)/ Coupled Model Intercomparison Project Three (CMIP3) database (Meehl *et al.* 2007), which offers references for the models at its website (http://www-pcmdi.llnl.gov/ipcc/model_documentation/ipcc_model_documentation.php). The model list is given in Table 1, including their short names used in this paper. The first 24 models are taken from the IPCC-AR4/CMIP3 database managed by PCMDI. In addition to these 24 models, we make use of the HadOPA model that is not part of the IPCC-AR4, but has been shown in several studies to display a realistic evolution and mechanisms in its onset and termination phase (Lengaigne *et al.* 2004; Lengaigne et al. 2006). For all the models, the sea surface temperature (SST), the zonal wind stress (τ_x) and the precipitation (Pr) were analysed. In addition, the depth of the 20°C when available has been used as a proxy of the thermocline depth in the equatorial Pacific.

In this study, we wish to focus on the internal variations of the coupled climate model systems, without introducing added complexity of changes in radiative forcing. We therefore study the set of experiments in which radiative forcing (and land use) is held at constant, pre-industrial values – this set of runs is referred to as the "Pre-Industrial Control" or picntrl experiments. However, the basic El Niño properties and the conclusions drawn from this study are not significantly altered if we explore the "Present-day Control" (pdcntrl) or the "Climate of the 20th century" (20c3m) experiments. The 25 datasets are interpolated (2-D linear

interpolation) onto a common 2.5° longitude by 2.5° latitude grid. Monthly anomalies are calculated by removing a mean climatological cycle, and a 5-month running mean is applied to the anomalies in order to focus on interannual variations in tropical climate conditions.

2.2. *Diagnosing moderate and extreme El Niño events in CGCMs*

El Niño amplitude in CGCMs is first diagnosed by calculating the SST anomalies (SSTA) averaged over the Niño3.4 region (170°-120°W, 5°N-5°S), which is often used in observations to identify El Niño events. The monthly standard deviation (σ) of Niño3.4 SSTA is shown in Table 1 for each model, and highlighting the large spread in the simulated ENSO amplitude ranging from 0.15 for GISS-AOM to 1.81 for the IAP-FGOAL. The inter-model variability of σ largely recovers the relative amplitudes of ENSO variability across the models as reported in the more comprehensive studies of ENSO in this set of models (Leloup et al. 2008; Guilyardi 2006; Van Oldenbourgh *et al.* 2005).

To objectively identify and quantitatively describe the evolution of El Niño events in this database, we use a criterion similar to the one introduced by Trenberth (1997): an El Niño event is defined for each dataset as a period where the Niño3.4 time series exceed $\sigma/2$ during at least six consecutive months (the events selected with this method is not very sensitive to slight modifications of the event duration criterion). As we aim to contrast the termination of extreme and moderate El Niño events, we need an objective criterion to distinguish between these two types of events. As discussed in the introduction, a peculiar feature for extreme El Niño events (e.g. 1982-83 and 1997-98) is the displacement of the warm-pool and associated convective activity from the central to the eastern part of the equatorial Pacific in winter at the height of the event. Figure 3 display a scatter plot of the maximum (minimum) EPAC precipitation anomalies

vs. the corresponding EPAC SSTA for each El Niño (La Niña) event. As expected, the precipitations show a nonlinear response to SSTA for very warm conditions over the 1957-2001 period. All La Niña events and most of the El Niño events display a rather weak precipitation response to SSTA. This is only for the two strongest El Niño events (1982-83 and 1997-98) that intense rainfall occurs in the EPAC. Whereas most of the models display a nearly linear relationship between precipitation and SST anomalies (INMCM, BCCR, CSIROs, CCMAs, …), 4 models (MPI, GFDL-1, CNRM, HadOPA) reproduce a clear nonlinear relationship with their warmest El Niño events associated with the onset of convective activity in the EPAC (other panels on Fig. 3). As for observations, these strong precipitations mainly occur in DJF or MAM (i.e. during the peak and termination phase). The SSTA threshold related to the onset of convection depends on the models (e.g. 4°C for MPI and 2.5°C for HadOPA). To use a common criteria for observations and all models, we thus define as extreme El Niño events those in which atmospheric deep convection develops in the EPAC such that precipitation anomalies in the equatorial eastern Pacific (120-90°W, 0°) exceed a 4mm/day precipitation anomaly threshold during the event. Using this method, the 1997-98 and 1982-83 events falls into this category whereas all the other events during the 1957-2001 period are identified as moderate events. Among the models, only six of them are able to simulate extreme El Niño events (HadOPA, CNRM, MPI, GFDL-1, MIUB and HadCM3). As only two extreme events develop in the MIUB and HADCM3 models, we will focus in the following on the evolution of El Niño events in the 4 remaining models. These models are among those that display the strongest Niño3.4 SST standard deviation. However, the IAP model that simulates the strongest ENSO variability do not simulate extreme El Niño events – this may be in part due to the very strong equatorial Pacific cold SST bias exhibited by this model, which keeps the warmest SSTs off equator even under extreme El Niño SST anomalies.

In the following, we will restrict our analysis to the events that reach their maximum amplitude in boreal fall or winter (September-February). We do so because of our focus on the termination of El Niño events, which has been shown in the observations to display a strong seasonal phase locking, with most of the observed El Niño events maturing during fall and winter time (Harrison and Larkin 1998). For example, over the 1957-2001 period, 86% of the events in the Hadley Center SST data (HadISST, Rayner et al 2003) peak in boreal fall or winter. As the interaction of El Niño with the annual cycle has been recognised as a fundamental cause of this phase locking (e.g. Tziperman et al. 1997; An and Wang 2001; Vecchi and Harrison 2003, Lengaigne et al 2006), we wish to consider this seasonal phase locking when building El Niño composites. For each model, the percentage of events occurring in boreal fall and winter seasons are indicated in Table 1. Most of the models underestimate the percentage of El Niño events peaking during these seasons. However, some of the models are able to recover the seasonal tendency in their simulated El Niño events (*e.g.,* HadOPA, CNRM-CM3, IAP, MIUB, HADCM3). These models are characterized by a relatively strong ENSO variability. In contrast, other models (CSIRO-5, CSIRO-0, GISS-EH, HADGEM1) display no seasonal phase locking.

Figure 4 contrasts the evolution of extreme and moderate El Niño events (as defined previously), showing equatorial SSTA Time-Longitude diagrams for extreme and moderate El Nino composites for the four models considered (HadOPA, CNRM, MPI, GFDL-1). First, as expected, the average amplitude of extreme events is two- to three-times larger than that of moderate one. With regards to the spatial location of the SSTA, extreme and moderate El Niño development phase (Year(0)) are relatively similar within each model, with maximum positive SSTA located at the El Niño onset in the eastern part of the basin for CNRM, MPI and GFDL1 and in the central part for HadOPA. As expected, SSTAs mature in fall-winter season for all models and events. Thought the El Niño development and peak phases have similar SSTA

patterns for extreme and moderate El Niño events within each model (although not of the same amplitude), the SSTA structure clearly differs during their termination. For moderate events, SSTA anomalies start decaying in spring of Year(+1) in the EPAC with a shift into "La Niña-like" conditions around May-June. In contrast, extreme El Niño events display persistent positive SSTA in the EPAC that last well into boreal spring, along with an abrupt decay of the SSTA in early summer (May to July, depending on the models). This behavior is qualitatively similar to the observed termination of the extreme and moderate El Niño events, as displayed on Figure 1a-b.

2.3. Coupled mechanisms involved in the extreme and moderate El Niño termination

To explore the mechanisms at play in the termination of moderate and extreme El Niño events in these models, Figure 5 contrasts the evolution of the SST and thermocline depth anomalies in the EPAC, and the near dateline zonal wind stress anomalies for the two types of events in each model. The termination of moderate El Niño events in these models can be easily understood by analyzing the evolution of the EPAC thermocline depth (only available for three of the four models). For these events, positive thermocline depth anomalies reach their maximum amplitude in winter (December-January) and rapidly decay from then on (Fig. 5e-g). This reduction in the thermocline depth directly decreases the SST by changing the temperature of the water upwelled and mixed vertically into the oceanic mixed layer. SSTs return to near-normal values around May (Fig. 5a-d).

The EPAC thermocline shoaling follows, and is likely driven by, the strong decrease of the positive near-Dateline equatorial zonal wind stress anomalies beginning November of Year(0) occurring in all models and El Niño types (Fig. 5h-k). Several studies based on observations (Harrison and Larkin 1998; Harrison and Vecchi 1999; Vecchi and Harrison 2003) and models

results (Spencer 2004; Vecchi 2006; Lengaigne *et al.* 2006) have suggested that meridional changes in coupled ocean-atmosphere system are a principal mechanism for this central equatorial Pacific wind forcing decrease in winter. This scenario is motivated by the robust presence of a southward shift of the near-Dateline westerly zonal wind stress anomalies associated with El Niño (Fig. 2), which results in a weakening of the near-equatorial zonal stress.

Figure 6 shows the evolution of the meridional structure of near-date-line wind anomaly field for simulated El Niño events. As in the observations, this characteristic southward shift of zonal wind stress occurs for all models from November of the Year(0). This southward shift of the wind acts to reduce the strength of the equatorial westerlies near the Dateline, which results in a shoaling of the EPAC thermocline through eastward-propagating Kelvin pulses, and preconditions the termination of the El Niño events.

The mechanisms controlling the termination of extreme El Niño events exhibit further complexity, though some commonalities exist with those behind the termination of moderate events. As with the moderate events, in late autumn of extreme El Niño events there is a decrease of the central equatorial Pacific zonal wind stress associated with a southward shift of the westerlies (Fig. 5h-k and Fig. 6); the central equatorial Pacific wind changes are followed by a rapid thermocline shoaling in the EPAC (Fig. 5e-g).

However, in contrast to moderate events, this southward wind shift and thermocline shoaling is not followed by a cooling in the EPAC (Fig. 5a-d). For these extreme events, the EPAC SSTAs remain significantly warmer than normal during the spring season while thermocline shoals. Then, in May-July, an abrupt and rapid SST cooling occurs, while the thermocline depth has already been very close to its climatological conditions for some time. This prolonged warming is not readily understood in terms of the evolution of the EPAC thermocline in isolation. This peculiar period is characterized by a decoupling of the typically

strong connection between SSTA and thermocline depth in the EPAC (Harrison and Vecchi 2001; Zelle *et al.* 2003; Zhang and McPhaden 2006).

To understand the period of shallow thermocline and warm SSTA at the end of extreme El Niño events, we must explore local atmospheric changes. The very warm SST anomalies that develop for very strong El Niño events (about +4°C) are associated with the development of strong precipitation anomalies in the eastern Pacific in winter (Fig. 7a-d). The establishment of a strong convective activity is accompanied by a relaxation of the trade winds in the EPAC (Fig. 7e-h). Thus, the weakening of EPAC easterlies leads to a reduction of wind-driven upwelling and mixing, and decouples the mixed-layer from the subsurface in the EPAC. Even as the thermocline shoaling beginning in December brings cold water closer to the surface, the relaxation of the local easterlies isolates the oceanic mixed layer from these waters. This peculiar situation (shallow thermocline, warm SSTs, equatorial convection and reduced easterlies) lasts until late spring/early summer when the seasonal reinforcement of the easterlies rapidly cools the surface, ending the El Niño event with an SSTA decay as strong as 2°C/month. During moderate events, on the other hand, the EPAC SSTA are not warm enough to allow the development of equatorial convection (Fig. 7a-d) in the eastern Pacific, keeping the zonal wind-stress anomalies relatively weak in the eastern Pacific (Fig. 7e-h) and wind-driven mixing and upwelling is able to connect the mixed layer with the subsurface as the thermocline shoals.

The development of this equatorial ITCZ during winter and spring for extreme El Niño events in these models is actually the signature of a southward shift of the ITCZ from its usual location north of the equator to the equatorial region. Figure 8 contrasts the evolution of extreme and moderate El Niño events in the eastern Pacific, showing Time-Latitude diagrams of SSTA, precipitation anomalies and warmest water edge for each of the considered models. The SST threshold defining the meridional extent of the warm pool differs among the models. In both

moderate and extreme El Niño events, the east Pacific SSTA is maximum on the Equator. However, the meridional location of the warmest east Pacific SST depends on the amplitude of the equatorial SSTA and the season. For moderate events, maximum SSTA reach 1-2°C in the EPAC. In this case, warmest SSTs remain located mainly north of the equator (5°N-15°N) with a tendency for all models to develop warm SST south of the equator during the spring season (the so-called double ITCZ problem). Thus, the warmest SST always remain out of the equatorial region during moderate El Niño events as the equatorial SSTA are not strong enough to reverse the meridional SST climatological gradient. As a consequence, strong atmospheric convection and precipitation remain located out of the equatorial region.

For extreme El Niño events, on the other hand, the equatorial SSTA in winter of about 4°C in the EPAC is strong enough to allow a meridional migration of the zone of maximum SST and convection close to the equator in January, leading to the relaxation of EPAC easterlies. Strong SSTA is maintained in the eastern Pacific until warmest SST and convective precipitations are shifted back north of the equator in relation with the seasonal march of insolation. As the equatorial easterlies strengthen the SSTA rapidly cools, terminating the El Niño in the eastern Pacific.

From this analysis, it appears that all models that are able to develop an equatorial ITCZ in the eastern Pacific during the mature phase of an El Niño event simulate a prolonged eastern Pacific warming that last until May-July of Year(+1). This equatorial ITCZ develops as the strong EPAC SSTA leads to the warmest water displacement from the northern hemisphere to the Equator, and to the development of equatorial convection. The mechanisms controlling this peculiar termination of extreme El Niño events in these models match those proposed in VH06 and V06 to explain the termination of the observed 1982-83 and 1997-98 El Niño events. These results demonstrate that state-of-the-art climate models are able to simulate the subtlety of this

termination and confirm that this peculiar termination character may be that expected to occur more generally in extreme El Niño events.

Interestingly, only models that display a larger than observed ENSO variability are able to simulated extreme events with intense precipitations in the eastern Pacific. This could be related to the cold bias in the equatorial cold tongue simulated in most of the CGCMs. EPAC SSTA therefore need to be stronger than in the observations to allow the onset of convection and the development of extreme El Nino events.

In the next section, we will discuss the implications of this peculiar termination of extreme El Niño events in terms of SST propagating signals.

3. **Implications to apparent propagation of El Niño:**

The zonal propagation characteristics of El Niño events are of interest because they may contain information pertaining to the dominant mechanisms controlling ENSO (*e.g.,* Trenberth and Stepaniak 2001; Fedorov and Philander 2001; Burgers and Van Oldenbourgh 2003; Guilyardi et al. 2006). In this section, we explore the impact of the different termination behavior between extreme and moderate El Niño events to their respective apparent propagation of SSTA, and discuss implications for the observed changes in propagation behavior and their interpretation.

As can be seen by contrasting the SSTA evolution in Figure 1.a and 1.b, and contrasting the evolution in the top panels of Fig. 4 with that in the bottom panels, extreme El Niño events exhibit a different apparent zonal propagation of their SSTA than do moderate events. Extreme El Niño events tend to exhibit an eastward propagation of SSTA, while moderate El Niño events exhibit a westward propagation. Comparing the time-longitude evolution of SSTA from moderate and extreme El Niño events in Figs. 1 and 4, it can be seen that there is little difference in

apparent propagation at the onset of the events, with the models and observations showing modest propagation (or in the case of the CNRM model a substantial westward propagation) of SSTA for both extreme and moderate El Niño events. However, the termination of the two kinds of events is characterized by fundamentally different propagation. Moderate events exhibit a rapid westward propagation of SSTA during their termination. Meanwhile, the termination of the observed extreme El Niño events is characterized by an apparent eastward propagation of the SSTA cooling, associated with the persistence of EPAC warm SSTAs for 3-4 months after the near-Dateline cooling has begun (around January of Year(+1)).

We can formalize the descriptive analysis of propagation characteristics described in the previous paragraph by exploring an index commonly used to describe zonal propagation of SSTA. The propagation characteristics of ENSO can be estimated using the running lag correlation of NIÑO3.4 to the Trans-Niño Index (or TNI, which measures the east-west zonal gradient of SSTA by taking the difference between the normalized SSTA in the Niño 1+2 region in the east and the normalized SSTA in the Niño4 region in the central west Pacific). The lagged correlation of TNI and NIÑO3.4 (with TNI leading NIÑO3.4) indicates the dominant direction of propagation of ENSO anomalies, with negative (positive) values indicating westward (eastward) propagation (Trenberth and Stepaniak 2001). The solid black line in Figure 9 shows the twenty-year running correlation of eight-month lagged TNI and NIÑO3.4 ($r_{8,20}$(TNI,NIÑO3.4)), which exhibited a change in sign in the mid-1970s (Trenberth and Stepaniak 2001). This indicates that the dominant propagation of ENSO SST anomalies went from westward to eastward across the mid-1970s.

The strength of the mid-1970s shift in apparent ENSO propagation was strongly influenced by the two extreme events of 1982-3 and 1997-8. This can be seen by the red line in Fig. 9, which shows the 7-year running correlation of eight-month lagged TNI and NIÑO3.4. The

two El Niño events were the dominant source of eastward propagation. In fact, the termination phases of these extreme El Niño events strongly influenced the character of the decadal $r_{8,20}$(TNI,NIÑO3.4). The dotted black line in Fig. 9 shows the result of computing $r_{8,20}$(TNI,NIÑO3.4) without the termination phases of the 1982-3 and 1997-8. Without the termination of the extreme El Niño events of 1982-3 and 1997-8, the mid-1970s shift in $r_{8,20}$(TNI,NIÑO3.4) disappears and a smoother decadal reduction in the negative amplitude of $r_{8,20}$(TNI,NIÑO3.4) is seen.

Figure 10 shows that three of the four climate models (HadOPA, MPI, GFDL1) exhibit a strong influence of the termination of extreme El Niño events on the apparent propagation characteristics of ENSO (as computed using $r_{8,20}$(TNI,NIÑO3.4)), similar to that seen since the mid-1950s (Fig. 9). As for observations, each of these models display decadal changes in apparent propagation of SSTA and eastward propagating periods are associated with extreme El Niño events, and when these are removed (dotted lines), the overall. When removing Year(+1) of the simulated extreme El Niño events from TNI SSTA correlation, the overall propagation tends to be either stationary or westward. For example, for the MPI model, 3 periods of positive correlations for positive lags are seen during the 150 years of correlation (Years 0-20, 45-80 and 95-115 on Figure 10d). When we do not consider Year(+1) of the 4 extreme El Niño events during that period (identified by the arrows) in the lag-correlations calculations, these correlations reverse sign and could be interpreted as an eastward propagating signal. This confirms that the termination of one extreme event can be responsible on its own for a positive correlation period of about 20 years. Similar results are found for HadOPA and GFDL models with the disappearance or weaker positive correlation for positive lags when removing the termination of simulated extreme El Niño events.

Aspects of the propagation characteristics of ENSO are a therefore a consequence of the amplitude of the El Niño events, and the peculiar termination of extreme El Niño events. This analysis therefore suggest that the eastward SST propagating periods in models and observations deduced from the TNI-Niño34 lag-correlation can be to a large part attributed to the peculiar termination of few extreme El Niño events. Since aspects of the amplitude of extreme El Niño events are partly stochastically forced (*e.g.,* Lengaigne *et al.* 2003, 2004; Vecchi *et al.* 2006), the influence of the termination of extreme El Niño events may limit the usefulness of interpreting changes in $r_{8,20}$(TNI,NIÑO3.4) as an indication of changing large-scale deterministic dynamical constraints on ENSO. Calculating these lag-correlations over moving windows of 20-years period could artificially give the impression of long-term periods in which eastward propagation was dominant, when only a small subset of the events actually exhibited a dominant eastward propagation to their SSTs.

4. **Summary and discussion**

An assessment of global climate model simulations indicates that termination mechanisms for El Niño recently identified in observed data, involving meridional movements of atmospheric convections, are present in the climate models; this includes the processes that precondition the termination of El Niño events in general, and the mechanisms leading to a peculiar termination of extreme El Niño events (such as those of 1982-3 and 1997-8), in which the Eastern Equatorial Pacific (EPAC) warm anomalies persist well into boreal spring/early-summer in association with the development of an equatorially-centred ITCZ. The mechanisms controlling the peculiar termination of extreme El Niño events are consistent across the four models that exhibit extreme El Niño events and observational record, suggesting that they represent a general feature of

extreme El Niño events. Further, due to their unusual termination, extreme El Niño events exhibit an apparent eastward propagation of their SST anomalies, which can strongly influence estimates of the apparent propagation of ENSO over multi-decadal periods; the influence of extreme El Niño events on apparent propagation complicates interpretation of the physical mechanisms behind observed propagation changes.

Although El Niño events tend to be phase locked to the annual cycle and mature in amplitude in boreal winter (Trenberth 1997), the termination of El Niño events have been shown to vary from one event to another. Commonly, El Niño events terminate with EPAC SSTAs diminishing in winter so that SST in this area is near normal by early spring (Harrison and Larkin 1998). However, the termination of the two extreme 1982-83 -1997-98 have been shown to terminate unusually with warm EPAC SSTAs exceeding 4°C at the event peak and lasting well into boreal spring with a sharp decrease of the SSTAs in late spring-early summer (McPhaden 1999; Takayabu et al. 1999). An accurate simulation of the observed diversity of El Niño termination is important as these differences can have significant different climate impact. This study has evaluated the ability of 25 different state-of-the-art coupled ocean-atmosphere GCMs to simulate the termination of both moderate and extreme El Niño events.

We define extreme El Niño events as the events where atmospheric deep convection develops in the eastern Pacific, as it was the case for the two extreme observed events. Most of the CGCMs are unable to simulate the diversity of observed events. In their simulated events, convective anomalies never extend into the eastern Pacific. Only 4 models, characterized by a higher than observed ENSO variability, are able to simulate both type of events (HadOPA, MPI, GFDL-1, CNRM-CM3). For these models, simulated extreme events display a termination close to what observed in 1983 and 1998 with a prolonged eastern Pacific warming and a late decrease of the SSTAs late spring/early summer of Year(+1). In contrast, simulated moderate events

display a decay of SSTA anomalies in the eastern Pacific from late winter and a return to normal conditions in spring. This results confirms that the distinctive termination observed in 1983 and 1998 is that to be expected for extreme El Niño events in general.

In addition, we assessed the mechanisms responsible for the termination of moderate and extreme El Niño events in these 4 models. For moderate events, a late year southward shift of the near dateline zonal wind stress anomalies greatly decrease its equatorial component and drives an EPAC thermocline shallowing. This change in the thermocline depth directly decreases the SST with a return to near normal EPAC SST in late spring. For extreme El Niño events, the southward shift of the near dateline winds and the EPAC thermocline shallowing is also clear. However, the very warm SST anomalies that develop for very strong El Niño events are associated with the establishment of a strong convective activity in the eastern Pacific accompanied by a relaxation of the trade winds in that region. Even if the thermocline shallowing in winter makes cold water available, the strong relaxation of the easterlies decouple the surface and the subsurface in the eastern equatorial Pacific because there is a reduced wind-forced upwelling. This situation lasts until late spring/early summer when the seasonal reinforcement of the easterlies rapidly cools the surface, ending the El Niño event with a rapid SSTA decay in early summer.

Extreme and moderate El Niño events exhibit distinct equatorial SSTA zonal propagation characteristics. Because warm SSTA persists in the EPAC for extreme El Niño events, while the central Pacific cools – partly through upwelling driven by strong cross-equatorial winds (e.g., Picaut et al. 2002) – extreme El Niño events exhibit a strong eastward propagating SSTA signal at their end in both models and observations (e.g., Fig.1 and Fig.4). Meanwhile, moderate El Niño events have strong EPAC easterly trade winds through their end phase, so EPAC SSTA cools as the thermocline shoals – thus giving them a dominantly westward propagation of SSTA at their end. We have shown that a single extreme El Niño event can influence estimates of

apparent zonal SSTA propagation over twenty years (Section 4), both in observations and the climate models. Using a commonly used estimate of propagation (lagged correlation of TNI and NIÑO3.4, e.g., Trenberth and Stepaniak 2001; Guilyardi 2006), an extreme El Niño event can make it seem that the period was characterized by eastward propagation, though the signal is dominated by the end-phase of a single event. Thus, an accurate interpretation of apparent propagation of SSTA must account for the impact of the termination of extreme El Niño events. Interpreting changes in the propagation of SST as evidence of changes in the underlying dynamical feedbacks behind El Niño (e.g., Guilyardi 2006; Guilyardi et al 2008) could be misleading, given the strong influence of the end of a single event.

The establishment of equatorial convection in the eastern part of the basin is actually a manifestation of a southward shift of the Intertropical Convergence Zone from the north to the equator. This study therefore underlines the importance of meridional processes tied to the seasonal cycle in the termination of El Niño events in CGCMs: the southward shift of near-Dateline westerly anomalies preconditions the termination of El Niño events, and the development/retreat of an equatorial ITCZ prolongs and abruptly terminates extreme El Niño events. The importance of the late year southward shift of the near-dateline zonal wind anomalies in reducing the central Pacific equatorial zonal wind anomalies and contributing to the El Niño termination has already been underlined in through observational analyses (Harrison and Vecchi 1999; Vecchi and Harrison 2003), forced model studies (Vecchi and Harrison 2006; Vecchi 2006; Spencer 2004) and coupled model experiments (Vecchi *et al.* 2004; Lengaigne *et al.* 2006; Xiao and Mechoso 2008). A series of model studies (Spencer 2004; Vecchi 2006; Lengaigne *et al.* 2006) underlined that the annual cycle of insolation accounts to a large part to the near-dateline southward shift of zonal winds. Another meridional process important in setting the timing in the extreme El Niño termination in the ITCZ is the southward shift of the ITCZ to the

equator in the eastern Pacific responsible for the prolonged warming along the western south-american coast. These results are consistent with recent work highlighting the importance of such a features in the peculiar termination of the 1997-98 event (Vecchi and Harrison 2006, Vecchi 2006).

- **Bibliography:**

An S-I, Wang B (2001) Mechanisms of Locking El Niño and La Niña Mature Phases to Boreal Winter. J Clim 14:2164-2176

Belamari S, Redelsperger J-L, Pontaud M (2003) Dynamic Role of a westerly wind burst in triggering an equatorial Pacific warm event. J. Clim 16:1869-1890

Boulanger J-P, Menkes C, Lengaigne M (2004) Role of high-frequency wind variability and other potential mechanisms in the onset, growth and termination phases of the 1997-1998 El Niño. Clim Dyn 22 :267-280. Doi :10.1007/s00382-003-0383-8

Burgers G, van Oldenborgh GJ (2003) On the impact of local feedbacks in the Central Pacific on the ENSO cycle. J Clim 16:2396-2407

Federov AV, Philander SG (2001) A stability analysis of tropical ocean-atmosphere interactions: Bridging measurements and theory for El Niño. J Clim 14:3086-3101

Giese BS, Harrison DE (1990) Aspects of the Kelvin wave response to episodic forcing. J Geophys Res 95 :7289-7312

Giese BS, Harrison DE (1991) Eastern equatorial Pacific response to three composite westerly wind types. J Geophys Res 96:3239-3248

Guilyardi E, (2006) El Niño- mean state - seasonal cycle interactions in a multi-model ensemble. Clim Dyn 26:329-348. Doi: 10.1007/s00382-005-0084-6

Guilyardi E, Wittenberg A, Fedorov A, Collins M, Wang C, Capotondi A, van Oldenborgh GJ, Stockdale T (2008) Understanding El Niño in Ocean-Atmosphere General Circulation Models : progress and challenges. Bull. Amer. Met. Soc., published online, in press.

Harrison DE, Vecchi GA (1997) Westerly wind events in the tropical Pacific, 1986-1995. J Clim 10 :3131-3156

Harrison DE, Larkin NK (1998) Seasonal U.S. temperature and precipitation anomalies associated with El Niño: Historical results and comparison with 1997–1998. Geophys Res Lett 25:3959–3962

Harrison DE, Vecchi GA (1999) On the termination of El Niño. Geophys Res Lett 26:1593-1596

Harrison DE, Vecchi GA (2001) El Niño and La Niña—Equatorial Pacific Thermocline Depth and Sea Surface Temperature Anomalies, 1986-98. Geophys Res Lett 28:1051–1054

Leloup J, Lengaigne M, Boulanger J-P (2008) Twentieth century ENSO characteristics in the IPCC database. Clim Dyn 30:277-291. Doi: 10.1007/s00382-007-0284-3

Lengaigne M, Boulanger J-P, Menkes C, Masson S, Madec G, Delecluse P (2002) Ocean Response to the March 1997 Westerly Wind Event. J Geophys Res 107:8015. Doi:1029/2001JC000841

Lengaigne M, Boulanger J-P, Menkes C, Madec G, Delecluse P, Guilyardi E, Slingo JM (2003) The March 1997 Westerly Wind Event and the onset of the 1997/98 El Niño: Understanding the atmospheric response. J Clim16:3330-22243

Lengaigne M, Guilyardi E, Boulanger J-P, Menkes C, Delecluse P, Inness P, Cole J, Slingo JM (2004) Triggering of El Niño by Westerly Wind Events in a Coupled General Circulation Model. Clim Dyn 23:601-620. Doi: 10.1007/s00382-004-0457-2

Lengaigne M, Boulanger JP, Menkes C, Spencer H (2007) Influence of the seasonal cycle on the termination of El Nino events in a Coupled General Circulation Model. J Clim 19:1850–1868. Doi: 10.1175/JCLI3706.1

McPhaden MJ, Zebiak SE, Glantz MH (2006) ENSO as an Integrating Concept in Earth Science. Science 314:1740. Doi: 10.1126/science.1132588

McPhaden MJ (1999) Genesis and evolution of the 1997-98 El Niño. Science 283:950-954.

Neelin JD, Battisti DS, Hirst AC, Jin FF, Wakata Y, Yamagata T, Zebiak SE (1998) ENSO theory. J Geophys Res 103:14261-14290

Picaut J, Hackert E, Busalacchi AJ, Murtugudde R, Lagerloef GSE (2002) Mechanisms of the 1997–1998 El Niño–La Niña, as inferred from space-based observations, J Geophys Res 107:3037. Doi:10.1029/2001JC000850

Rasmusson EM, Carpenter TH (1982) Variations in tropical sea surface temperature and surface wind fields associated with the Southern Oscillation/El Niño. Mon Wea Rev 110:354-384

Rayner NA, Parker DE, Horton EB, Folland CK, Alexander LV, Rowell DP, Kent EC, Kaplan A (2003) Global analyses of sea surface temperature, sea ice, and night marine air temperature since the late nineteenth century. J Geophys Res 108:4407. Doi:10.1029/2002JD002670

Spencer H (2004) Role of the Atmosphere in the Seasonality of El Niño. Geophys Res Lett 31:24104. Doi: 10.1029/2004GL021619

Takayabu YN, Iguchi T, Kachi M, Shibata A, Kanzawa H (1999) Abrupt termination of the 1997-98 El Nino in response to a Madden-Julian oscillation. Nature 402:279-282

Trenberth KE (1997) The definition of El Niño. Bull Amer Met Soc 78: 2771-2777

Trenberth KE, Stepaniak DP (2001) Indices of El Niño evolution. J Clim 14:1697-1701

Tziperman E, Zebiak S, Cane MA (1997) Mechanisms of seasonal - ENSO interaction. J Atmos Sci 54:61-71

van Oldenborgh G, Philip S, Collins M (2005) El Niño in changing climate: a multi-model study. Ocean Science 1:81-95

Vecchi GA, Harrison DE (2000) Tropical pacific sea surface temperature anomalies, El Niño, and equatorial westerly wind events. J Clim 13:1814-1830

Vecchi GA, Harrison DE (2003) On the termination of the 2002-2003 El Niño event. Geophys Res Lett 30:1964. Doi :10.1029/2003GL017564

Vecchi GA, Harrison DE (2006). The termination of the 1997-98 El Niño. Part I: Mechanisms of Oceanic Change. J Clim 19:2633-2646

Vecchi GA (2006) The termination of the 1997-98 El Niño. Part II: Mechanisms of atmospheric change. J Clim 19:2647-2664

Wang C, Picaut J (2004) Understanding ENSO physics - A review (2004). In: Wang C, Xie SP, and Carton JA (ed) Earth Climate: The Ocean-Atmosphere Interaction. AGU Geophysical Monograph Series, pp 1–54.

Xiao H, Mechoso CR (2008) Seasonal cycle ENSO Interactions: Validation of Hypotheses. Submitted to J Clim

Zelle H, Appeldoorn G, Burgers G, van Oldenborgh GJ (2004) The Relationship between Sea Surface Temperature and Thermocline Depth in the Eastern Equatorial Pacific. J Phys Oceanogr 34:643–655

Zhang X, McPhaden MJ (2006) Wind Stress Variations and Interannual Sea Surface Temperature Anomalies in the Eastern Equatorial Pacific. J Clim 19:226–241

Figure captions:

Fig. 1 Time-Longitude diagram for extreme El Niño events (Year(0)=[1982, 1997]) of (a) equatorial SSTA (color), 28°C isotherm (thick line), (b) equatorial zonal wind stress anomaly (color), precipitation anomalies (lines) and (c) zonal wind stress (color). (d), (e) and (f): Idem for moderate El Niño events (Year(0)=[1963, 1965, 1969, 1972, 1976, 1977, 1979, 1987, 1991, 1994]). HadISST dataset (Rayner et al. 2004) is used for SST and ERA40 dataset is used for precipitation and wind stress.

Fig. 2 Time-Latitude diagram for (a) extreme El Niño events (Year (0)=[1982, 1997]) and (b) moderate El Niño events (Year(0)=[1963, 1965, 1969, 1972, 1976, 1977, 1979, 1987, 1991, 1994]) of near-Dateline zonal wind stress anomalies from the ERA40 analysis.

Fig 3 For the ERA40 analysis (upper left panel) and for each GCM listed in Table 1 (other panels, labeled with model name) a scatter plot of the maximum (minimum) eastern equatorial Pacific precipitation anomaly vs. the corresponding eastern equatorial Pacific SSTA for each El Niño (La Niña) events. Different symbols are used for different seasons: diamonds corresponds to DJF, triangles to MAM, squares to JJA and crosses to SON. Warm colors indicate El Niño events and cool colors indicate La Niña events. Notice that in observations and in many models the strongest precipitations in the eastern Pacific mainly occurs in DJF or MAM, and that the observations and four of the models (CNRM, MPI, GFDL-1 and HADOPA) show nonlinear response of eastern equatorial Pacific precipitation for very warm SSTA.

Fig. 4 Time-longitude evolution of the equatorial Pacific SSTA for (a-d) extreme and (e-h) moderate El Niño composites for 4 climate models (CNRM, MPI, GFDL-1 and HADOPA).

Fig. 5 Time evolution at the equator for extreme (back) and moderate (grey) El Niño composites of (a-d) SSTA, (e-g) 20°C isotherm depth anomalies in the equatorial eastern Pacific (120°W-90°W) and (h-k) zonal wind stress in the central Pacific (160°W-210°E) in 4 climate models (CNRM, GFDL-1, HADOPA and MPI).

Fig. 6 Time evolution at the equator for extreme (back) and moderate (grey) El Niño composites of (a-d) precipitation anomalies in the eastern Pacific (120°W-90°W) and (e-h) zonal wind stress anomalies in the eastern Pacific (140°W-90°W) in 4 climate models (CNRM, GFDL-1, HADOPA and MPI).

Fig. 7 Time-latitude evolution in the equatorial central Pacific (160°E-210°W) of zonal wind stress anomalies of (a-d) extreme and (e-h) moderate El Niño composites for 4 climate models (CNRM, GFDL-1, HadOPA and MPI).

Fig. 8 Time-latitude evolution in the equatorial eastern Pacific (120°W-90°W) of SSTA (color), 4mm/day isoline precipitation anomaly (solid line) and warm pool (dashed line) of (a-d) extreme and (e-h) moderate El Niño composites for 4 climate models (CNRM, GFDL-1, HadOPA and MPI). The warm pool edge is defined as the 25.5°C for CNRM, 27.5°C for MPI and GFDL-1 and 29.5°C for HadOPA.

Fig. 9 Eight-month lagged correlation of the Trans-Niño Index (TNI) with the normalized Niño34 SSTA over 1940-1995 period. Red line is for the 7-year running correlation, solid black line is for the 21-year running correlation and dotted black line is for the 21-year correlation with

the 1983 and 1998 years removed. Arrows at the top of the figure highlight the 1982-3 and 1997-8 El Niño events. Notice that the correlation is negative (indicating westward propagation) except for the influence of the two extreme El Niño events.

Fig. 10 Eight-month lagged correlation of the Trans-Niño Index (TNI) with the normalized Niño34 SSTA for (a) CNRM, (b) GFDL1, (c) HadOPA and (d) MPI models. Red line is for the 7-year running correlation, solid black line is for the 21-year running correlation and dotted black line is for the 21-year correlation with the Year(+1) of extreme El Niño events removed. Arrows at the top of the figure highlight extreme El Niño events El Niño events. Notice that the correlation is positive during periods including extreme El Niño events.

Table 1 The models considered in this study, their short names used throughout the paper and the length of the simulations (in years). The Niño34 SSTA standard deviation values (in °C), percentage of events peaking in the fall-winter seasons and the number of extreme and moderate El Niño events are also added. The rows in bold are those models used in the analysis of El Niño characteristics.

Figure 1

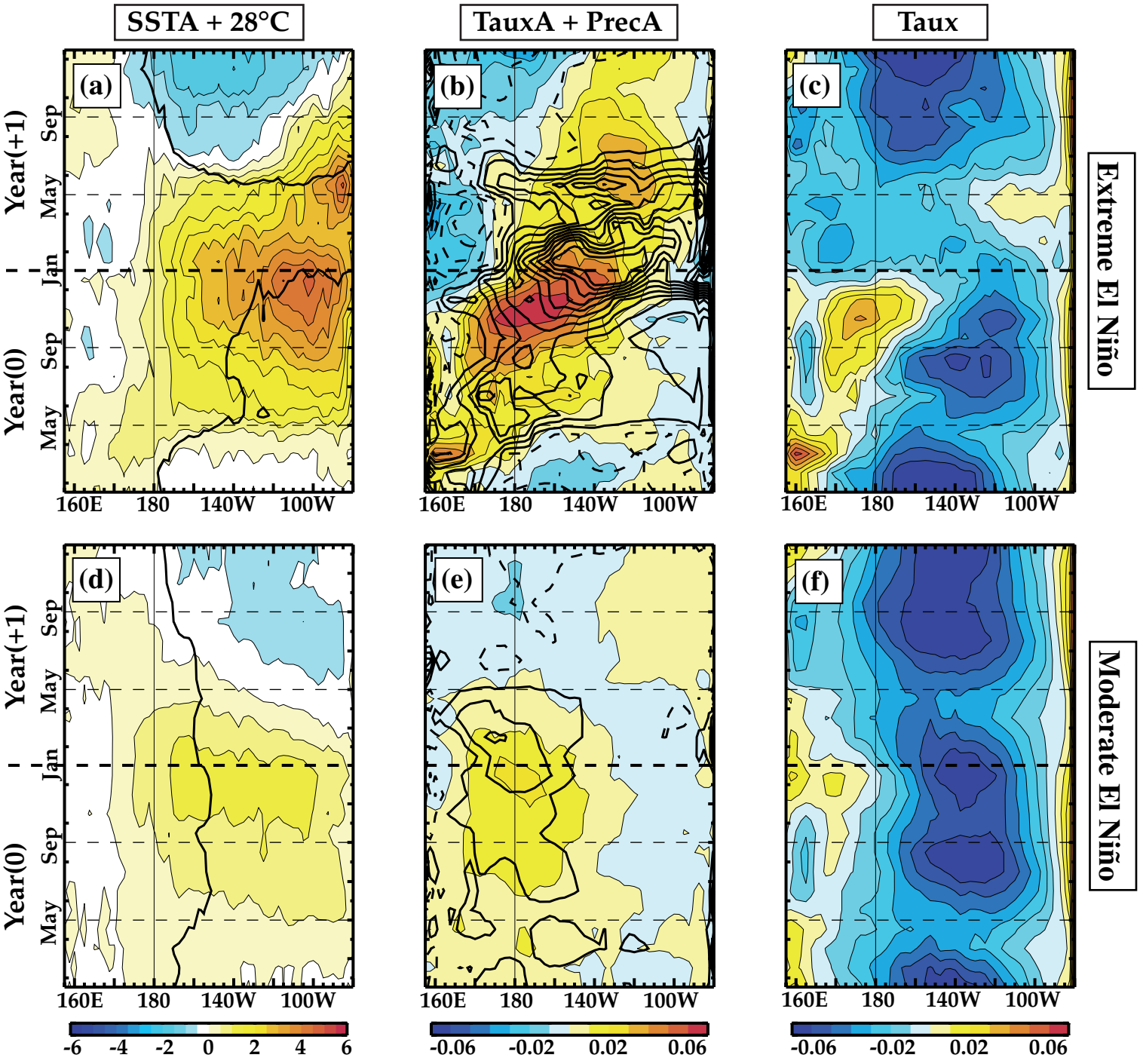

Fig. 1 Time-Longitude diagram for extreme El Niño events (Year(0)=[1982, 1997]) of (a) equatorial SSTA (color), 28°C isotherm (thick line), (b) equatorial zonal wind stress anomaly (color), precipitation anomalies (lines) and (c) zonal wind stress (color). (d), (e) and (f): Idem for moderate El Niño events (Year(0)=[1963, 1965, 1969, 1972, 1976, 1977, 1979, 1987, 1991, 1994]). HadISST dataset (Rayner et al. 2004) is used for SST and ERA40 dataset is used for precipitation and wind stress.

Figure 2

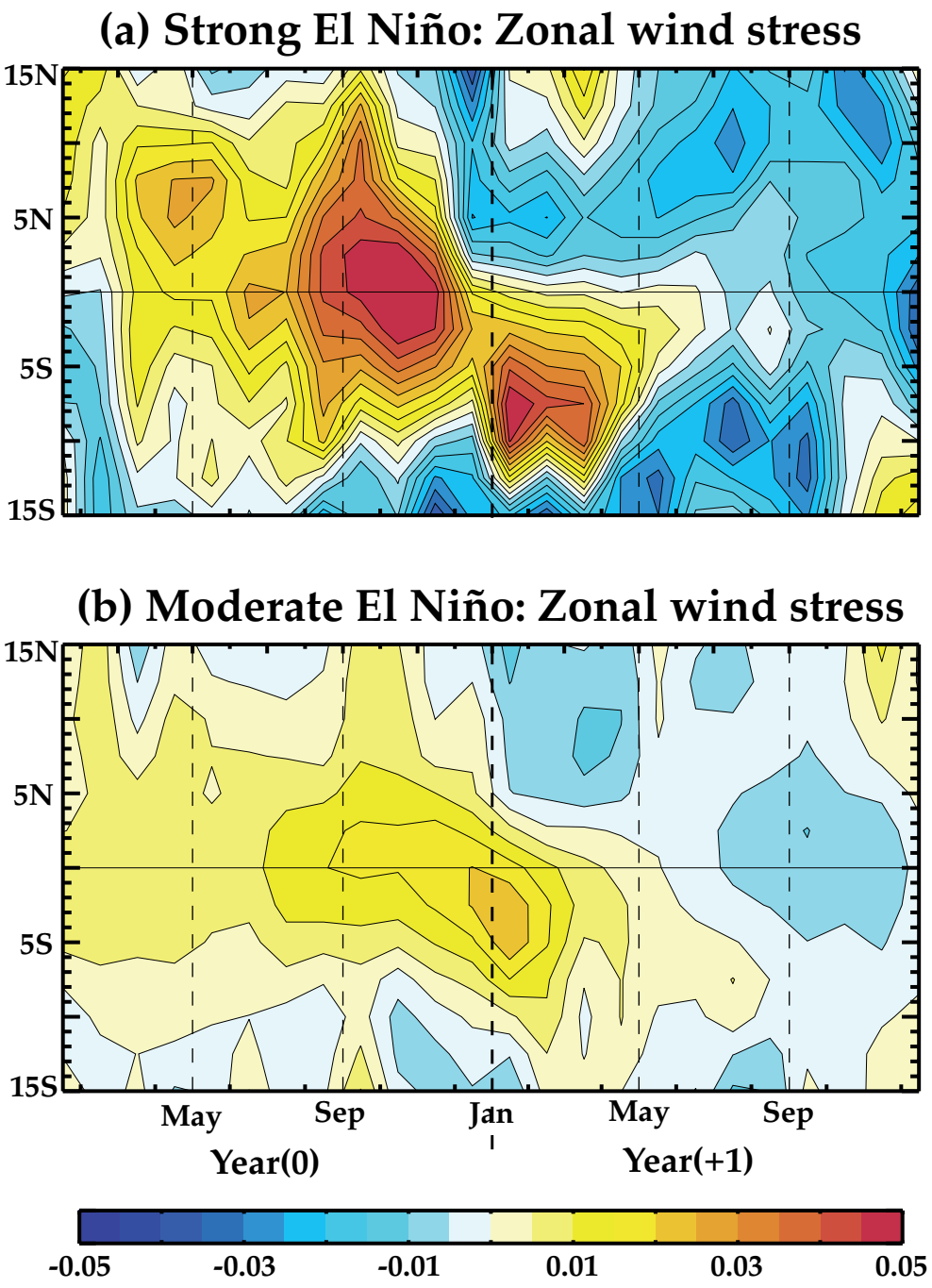

Fig. 2 Time-Latitude diagram for (a) extreme El Niño events (Year (0)=[1982, 1997]) and (b) moderate El Niño events (Year(0)=[1963, 1965, 1969, 1972, 1976, 1977, 1979, 1987, 1991, 1994]) of near-Dateline zonal wind stress anomalies from the ERA40 analysis.

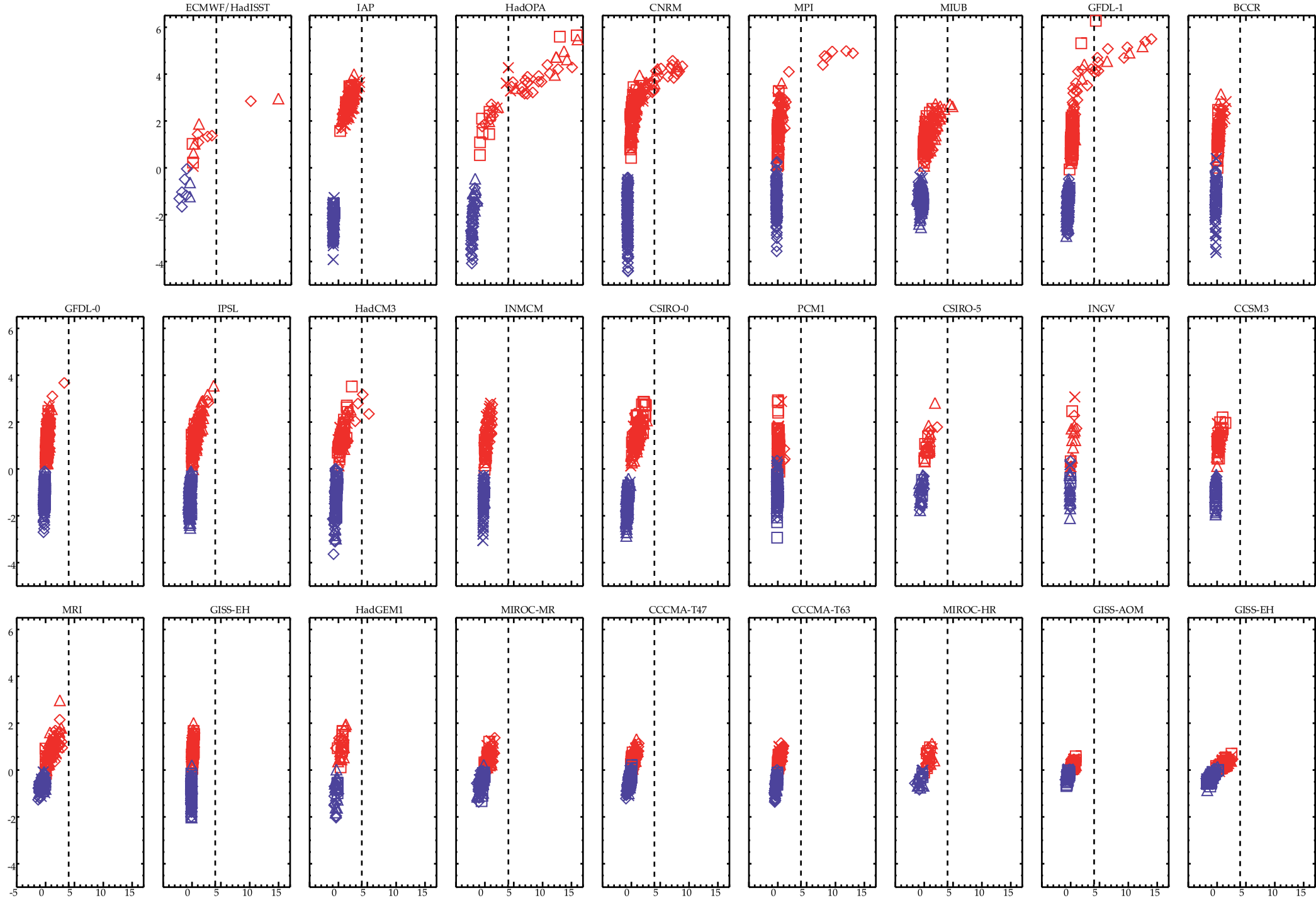

Figure 3 **Fig 3** For the ERA40 analysis (upper left panel) and for each GCM listed in Table 1 (other panels, labeled with model name) a scatter plot of the maximum (minimum) eastern equatorial Pacific precipitation anomaly vs. the corresponding eastern equatorial Pacific SSTA for each El Niño (La Niña) events. Different symbols are used for different seasons: diamonds corresponds to DJF, triangles to MAM, squares to JJA and crosses to SON. Warm colors indicate El Niño events and cool colors indicateLa Niña events. Notice that in observations and in many models the strongest precipitations in the eastern Pacific mainly occurs in DJF or MAM, and that the observations and four of the models (CNRM, MPI, GFDL-1 and HADOPA) show nonlinear response of eastern equatorial Pacific precipitation for very warm SSTA.

Figure 4

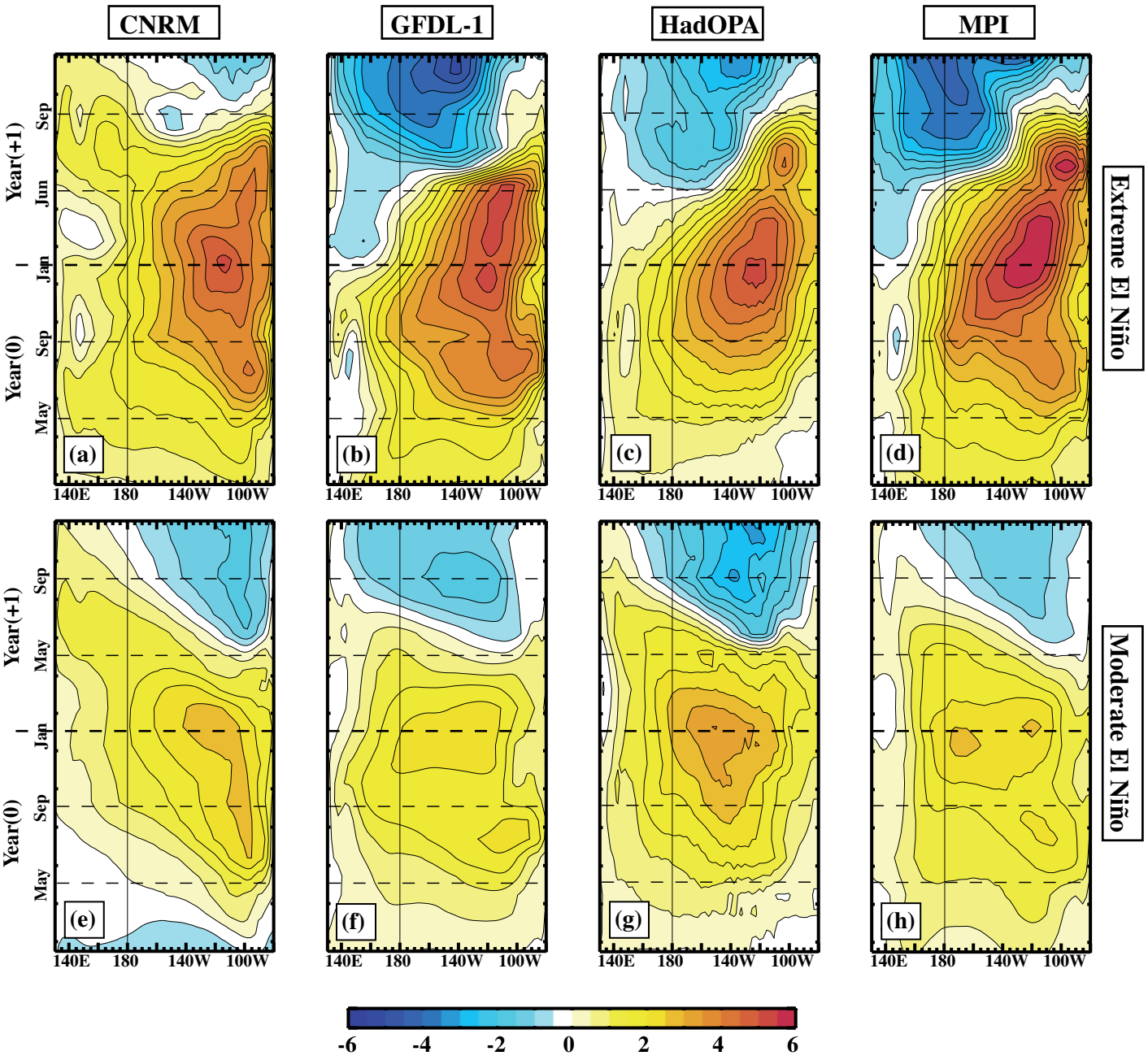

Fig. 4 Time-longitude evolution of the equatorial Pacific SSTA for (a-d) extreme and (e-h) moderate El Niño composites for 4 climate models (CNRM, MPI, GFDL-1 and HADOPA).

Figure 5

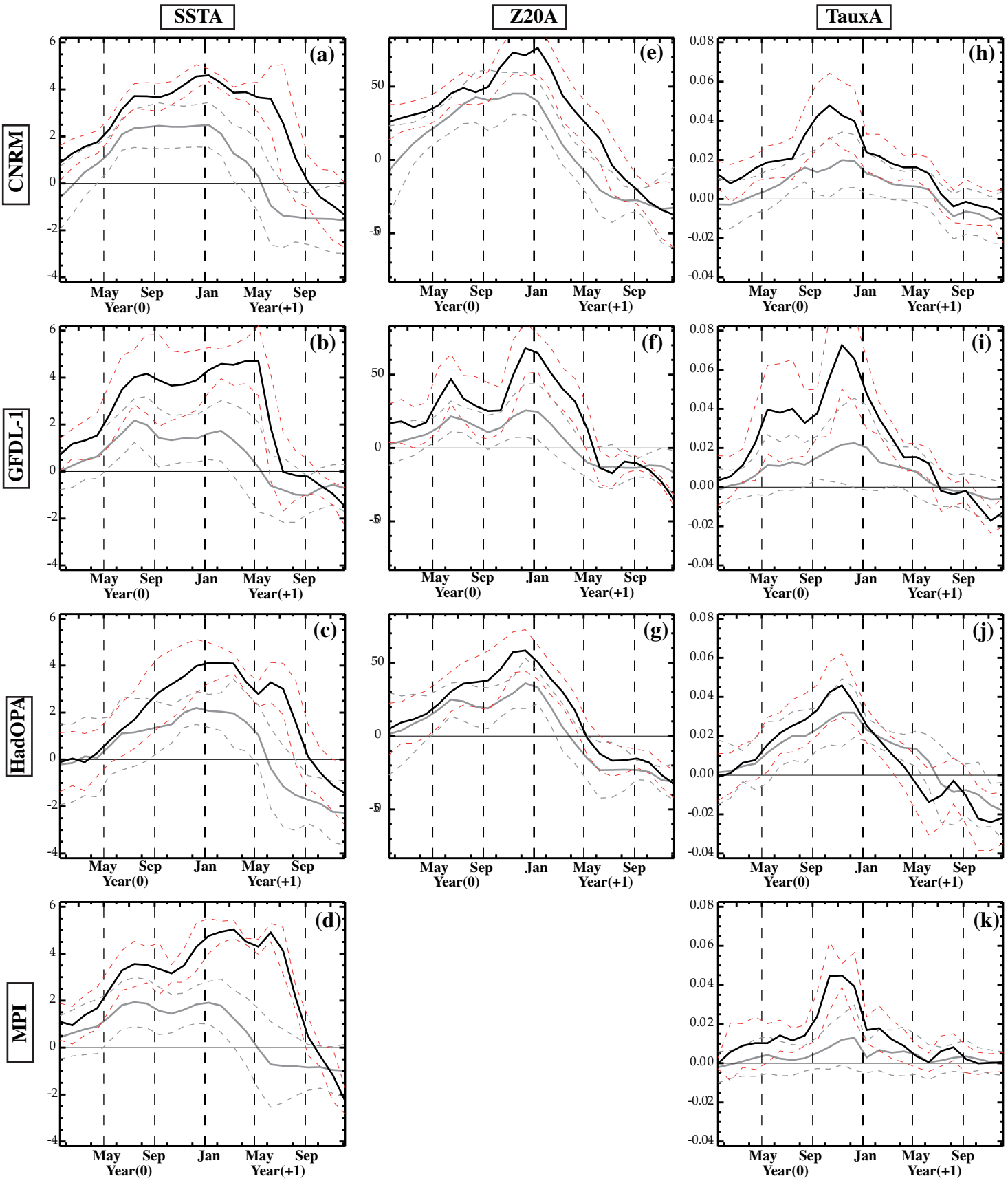

Fig. 5 Time evolution at the equator for extreme (back) and moderate (grey) El Niño composites of (a-d) SSTA, (e-g) 20°C isotherm depth anomalies in the equatorial eastern Pacific (120°W-90°W) and (h-k) zonal wind stress in the central Pacific (160°W-210°E) in 4 climate models (CNRM, GFDL-1, HADOPA and MPI).

Figure 6

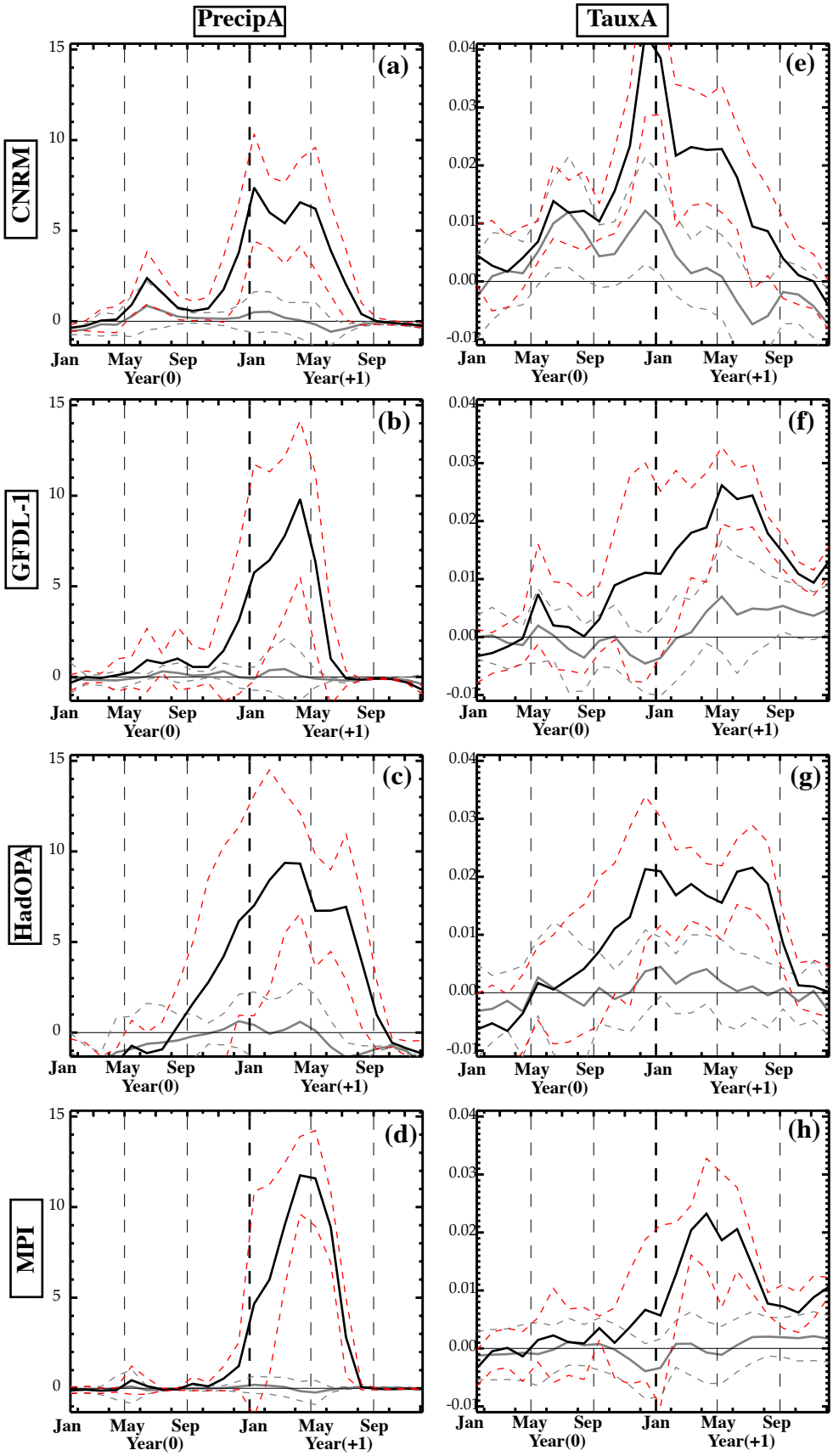

Fig. 6 Time evolution at the equator for extreme (back) and moderate (grey) El Niño composites of (a-d) precipitation anomalies in the eastern Pacific (120°W-90°W) and (e-h) zonal wind stress anomalies in the eastern Pacific (140°W-90°W) in 4 climate models (CNRM, GFDL-1, HADOPA and MPI).

Figure 7

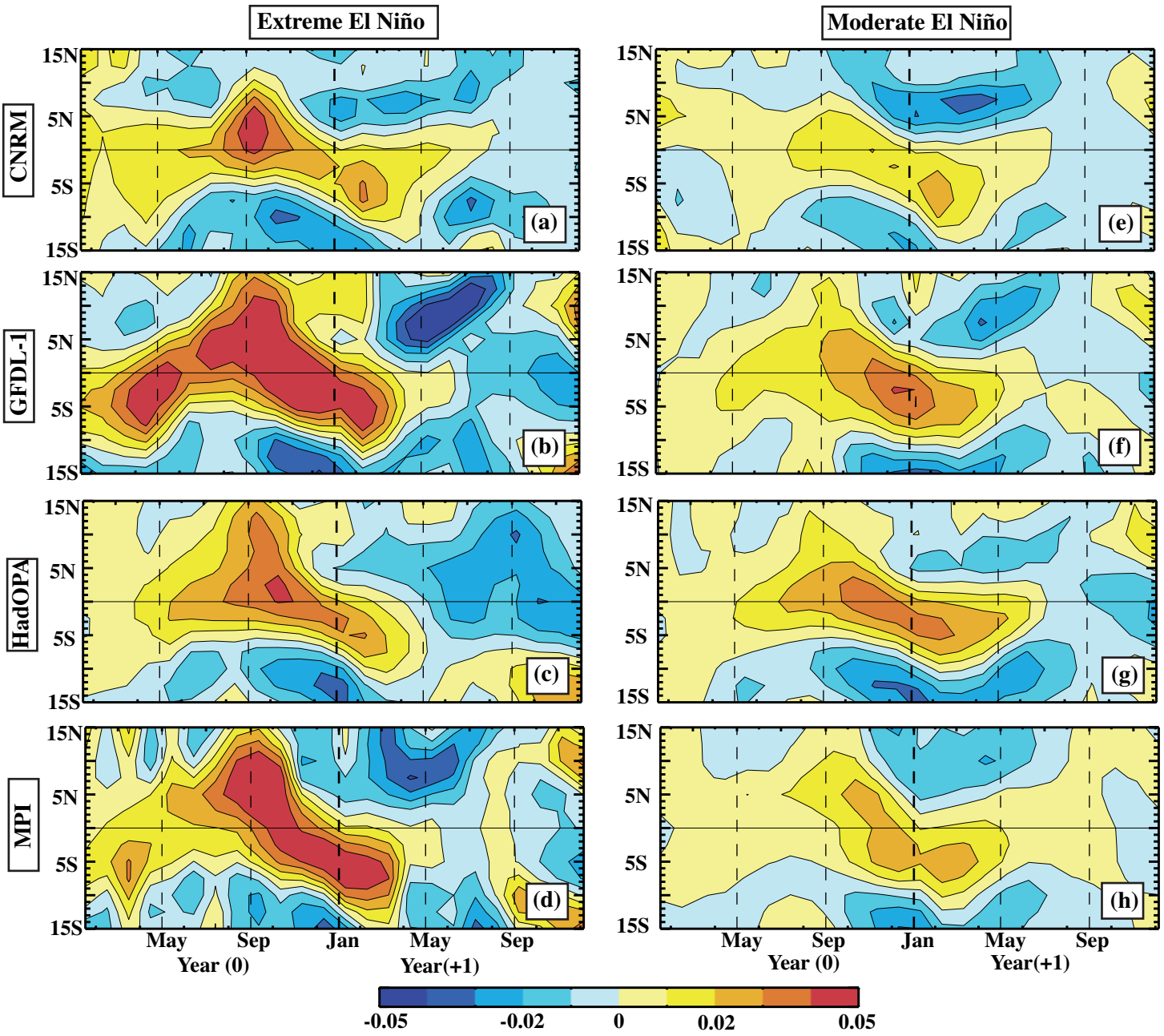

Fig. 7 Time-latitude evolution in the equatorial central Pacific (160°E-210°W) of zonal wind stress anomalies of (a-d) extreme and (e-h) moderate El Niño composites for 4 climate models (CNRM, GFDL-1, HadOPA and MPI).

Figure 8

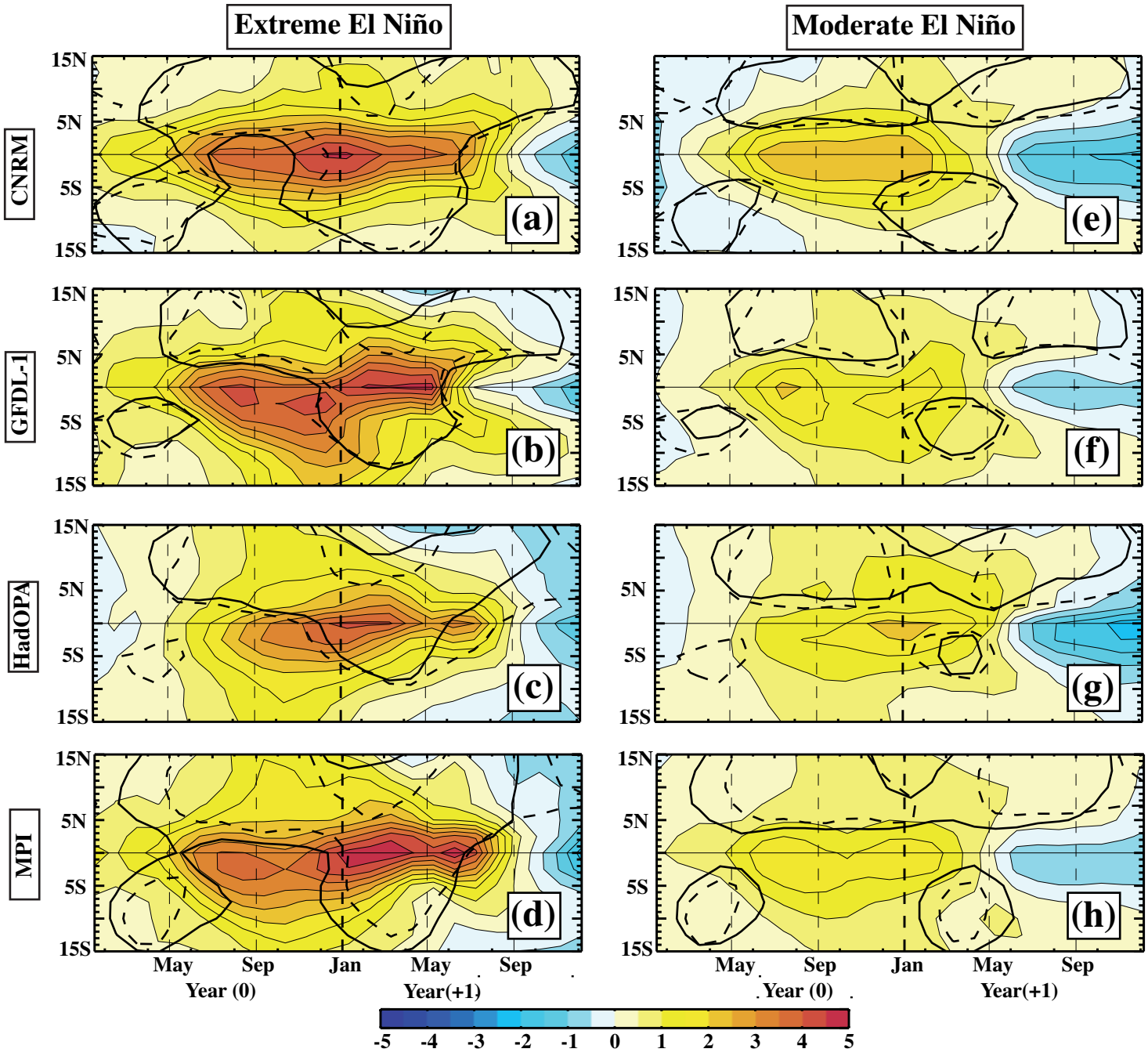

Fig. 8 Time-latitude evolution in the equatorial eastern Pacific (120°W-90°W) of SSTA (color), 4mm/day isoline precipitation anomaly (solid line) and warm pool (dashed line) of (a-d) extreme and (e-h) moderate El Niño composites for 4 climate models (CNRM, GFDL-1, HadOPA and MPI). The warm pool edge is defined as the 25.5°C for CNRM, 27.5°C for MPI and GFDL-1 and 29.5°C for HadOPA.

Figure 9

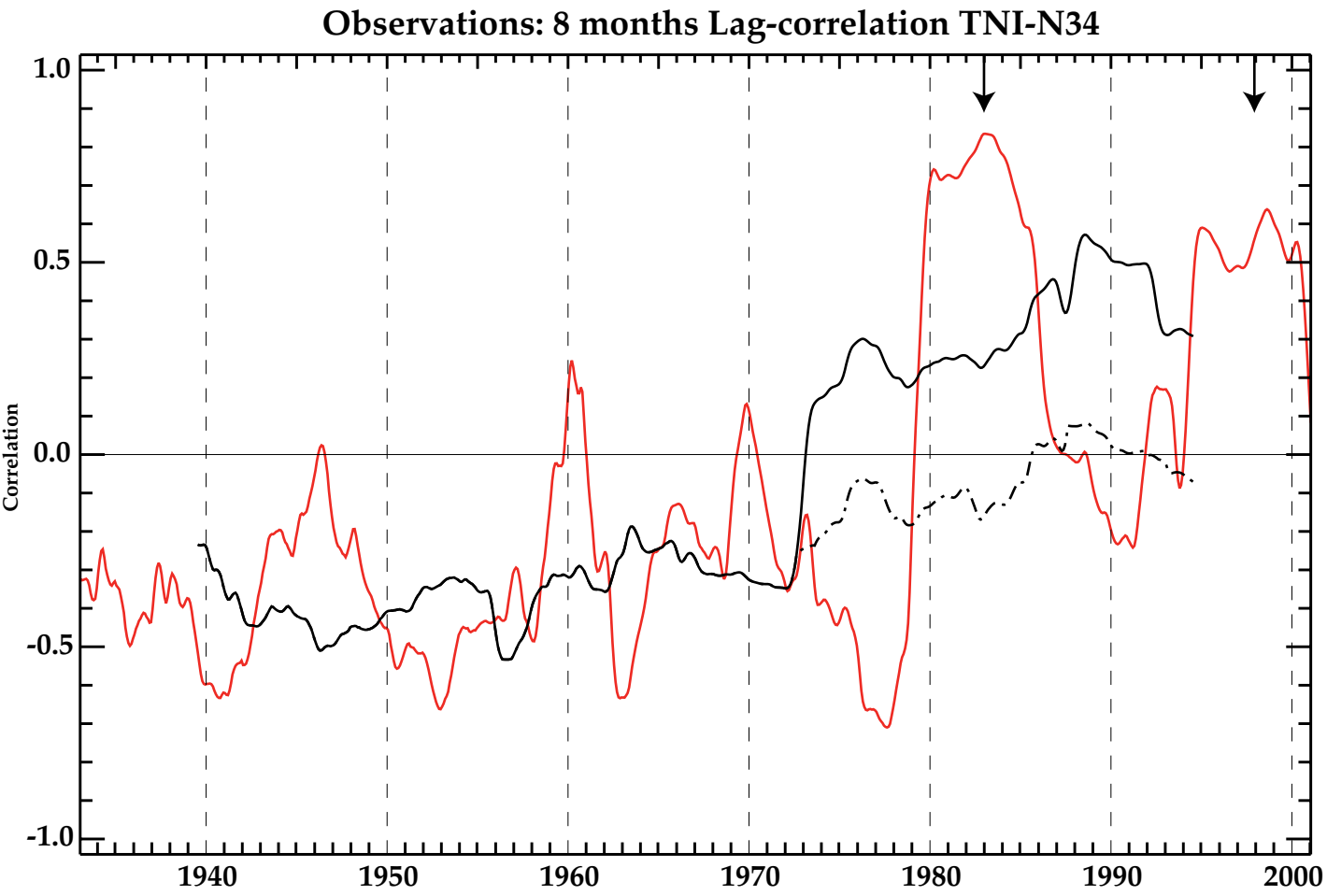

Fig. 9 Eight-month lagged correlation of the Trans-Niño Index (TNI) with the normalized Niño34 SSTA over 1940-1995 period. Red line is for the 7-year running correlation, solid black line is for the 21-year running correlation and dotted black line is for the 21-year correlation with the 1983 and 1998 years removed. Arrows at the top of the figure highlight the 1982-3 and 1997-8 El Niño events. Notice that the correlation is negative (indicating westward propagation) except for the influence of the two extreme El Niño events.

Figure 10

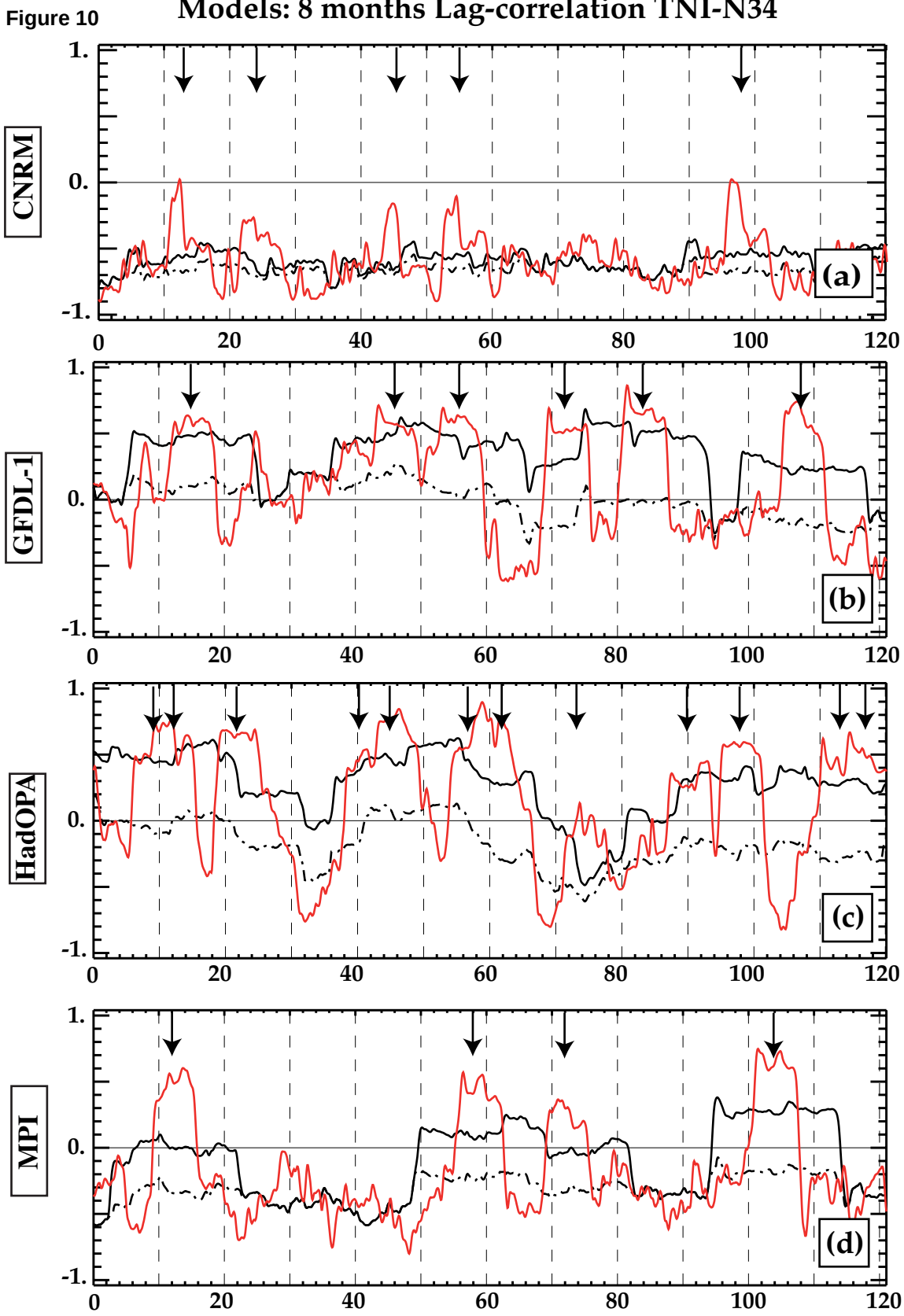

Fig. 10 Eight-month lagged correlation of the Trans-Niño Index (TNI) with the normalized Niño34 SSTA for (a) CNRM, (b) GFDL1, (c) HadOPA and (d) MPI models. Red line is for the 7-year running correlation, solid black line is for the 21-year running correlation and dotted black line is for the 21-year correlation with the Year(+1) of extreme El Niño events removed. Arrows at the top of the figure highlight extreme El Niño events El Niño events. Notice that the correlation is positive during periods including extreme El Niño events.

Table 1

DATA NAME	SHORT NAME	Simulation Length	$\sigma(SSTA_{Nino34})$	% of events peaking in fall-winter	Number of extreme-moderate events (peaking in fall-winter)
IAP−FGOALS-g1.0	IAP	350	1,81	94%	0-103 (0-97)
HadAM3-OPA	**HadOPA**	**190**	**1,67**	**98%**	**28-18 (28-17)**
CNRM−CM3	**CNRM**	**500**	**1,45**	**98%**	**17-138 (17-135)**
ECHAM5/MPI-OM	**MPI**	**505**	**1,22**	**67%**	**6-104 (6-68)**
MIUB−ECHO-G	MIUB	340	1,19	93%	2-136 (2-127)
GFDL−CM2.1	**GFDL−1**	**500**	**1,15**	**66%**	**14-88 (14-52)**
BCCR−BCM2.0	BCCR	250	0,90	71%	0-69 (0-49)
GFDL−CM2.0	GFDL−0	500	0,87	65%	0-139 (0-90)
IPSL−CM4	IPSL	500	0,86	65%	0-159 (0-103)
UKMO−HadCM3	HADCM3	340	0,84	79%	2-82 (2-64)
INM−CM3.0	INMCM	330	0,85	38%	0-80 (0-30)
HadISST (observations)	HadISST	45	0,82	84%	2-10 (2-8)
CSIRO−Mk3.0	CSIRO-0	380	0,82	58%	0-112 (0-65)
NCAR−PCM1	PCM1	350	0,81	58%	0-97 (0-56)
CSIRO−Mk3.5	CSIRO-5	130	0,77	52%	0-29 (0-15)
INGV−ECHAM4	INGV	100	0,71	65%	0-17 (0-11)
NCAR−CCSM3	CCSM3	130	0,75	68%	0-47 (0-32)
MRI−CGM2.3.2	MRI	350	0,70	73%	0-100 (0-73)
GISS−EH	GISS−EH	400	0,65	52%	0-101 (0-53)
UKMO−HadGEM1	HADGEM1	240	0,63	61%	0-64 (0-39)
MIROC3.2 (medres)	MIROC−MR	500	0,47	78%	0-89 (0-69)
CCCMA−CGCM3.1(T47)	CCCMA−T47	500	0,42	74%	0-128 (0-95)
CCCMA−CGCM3.1(T63)	CCCMA−T63	250	0,42	66%	0-88 (0-58)
MIROC3.2 (hires)	MIROC−HR	100	0,32	61%	0-23 (0-14)
GISS−ER	GISS−ER	500	0,17	53%	0-115 (0-61)
GISS−AOM	GISS−AOM	250	0,15	45%	0-65 (0-29)

Table 1: The models considered in this study, their short names used throughout the paper and the length of the simulations (in years). The Niño34 SSTA standard deviation values (in °C), percentage of events peaking in the fall-winter seasons and the number of extreme and moderate El Niño events are also added. The rows in bold are those models used in the analysis of El Niño